

# Compressive Sensing for Millimeter Wave Antenna Array Diagnosis

Mohammed E. Eltayeb, Tareq Y. Al-Naffouri, and Robert W. Heath, Jr.

**Abstract**—The radiation pattern of an antenna array depends on the excitation weights and the geometry of the array. Due to wind and atmospheric conditions, outdoor millimeter wave antenna elements are subject to full or partial blockages from a plethora of particles like dirt, salt, ice, and water droplets. Handheld devices are also subject to blockages from random finger placement and/or finger prints. These blockages cause absorption and scattering to the signal incident on the array, and change the array geometry. This distorts the far-field radiation pattern of the array leading to an increase in the sidelobe level and decrease in gain. This paper studies the effects of blockages on the far-field radiation pattern of linear arrays and proposes two array diagnosis techniques for millimeter wave antenna arrays. The proposed techniques jointly estimate the locations of the blocked antennas and the induced attenuation and phase-shifts. Numerical results show that the proposed techniques provide satisfactory results in terms of fault detection with reduced number of measurements (diagnosis time) provided that the number of blockages is small compared to the array size.

**Index Terms**—Antenna arrays, fault diagnosis, compressed sensing, millimeter wave communication.

## I. INTRODUCTION

THE abundance of bandwidth in the millimeter wave (mmWave) spectrum enables gigabit-per-second data rates for cellular systems and local area networks [1], [2]. MmWave systems make use of large antenna arrays at both the transmitter and the receiver to provide sufficient receive signal power. The use of large antenna arrays is justified by the small carrier wavelength at mmWave frequencies which permits large number of antennas to be packed in small form factors.

Due to weather and atmospheric effects, outdoor mmWave antenna elements are subject to blockages<sup>1</sup> from flying debris or particles found in the air as shown in Fig. 1. MmWave antennas on handheld devices are also subject to blockage from random finger placement and/or fingerprints on the antenna array. Blocking some of the antenna elements reduces the amount of energy incident on the antenna [3], [4]. For instance, it is reported in [5] that 90% of a 76.5 GHz signal

Mohammed E. Eltayeb and Robert W. Heath, Jr. are with the University of Texas at Austin, USA (emails: {meltayeb,rheath}@utexas.edu). Tareq Y. Al-Naffouri is with King Abdullah University of Science and Technology, Saudi Arabia (e-mail: tareq.alnaffouri@kaust.edu.sa). This research was partially supported by the U.S. Department of Transportation through the Data-Supported Transportation Operations and Planning (D-STOP) Tier 1 University Transportation Center and by the Texas Department of Transportation under Project 0-6877 entitled Communications and Radar-Supported Transportation Operations and Planning (CAR-STOP).

<sup>1</sup>The term blockage refers to a physical object partially or completely blocking a subset of antenna elements and should not be confused with mmWave channel blockage.

energy will be absorbed by a water droplet of thickness 0.23 mm. A thin water film caused by, for example a finger print, is also reported to cause attenuation and a phase shift on mmWave signals [5]. Moreover, snowflakes, ice stones, and dry and damp sand particles are reported to cause attenuation and/or scattering [3]-[7]. Because the size of these suspended particles is comparable to the signal wavelength and antenna size, random blockages caused by these particles will change the antenna geometry and result in a distorted radiation pattern [8], [9]. Random changes in the array’s radiation pattern causes uncertainties in the mmWave channel. Therefore, real time monitoring of mmWave antenna arrays is essential to ensure reliable communication links. This necessitates the design of reliable and low latency array diagnosis techniques that are capable of detecting the blocked antennas and the corresponding signal power loss and/or phase shifts caused by the blocking particles. Once a fault has been detected, pattern correction techniques proposed in [8]-[13] can be employed to calculate new excitation weights for the array.

Several array diagnostic techniques, which are based on genetic algorithms [14], [15], matrix inversion [16], exhaustive search [17], and MUSIC [18], have been proposed in the literature to identify the locations of faulty antenna elements. These techniques compare the radiation pattern of the array under test (AUT) with the radiation pattern of an “error free” reference array. For large antenna arrays, the techniques in [14]-[18] require large number of samples (measurements) to obtain reliable results. To reduce the number of measurements, compressed sensing (CS) based techniques have recently been proposed in [19] and [20]. Despite their good performance, the techniques in [14]-[20] are primarily designed to detect the sparsity pattern of a failed array, i.e. the locations of the failed antennas, and not necessarily blocked antennas. A suspended particle might, for example, only cause a phase shift on the signal incident on a subset of blocked antennas. The above diagnostic techniques will fail to detect this type of “partial blockage” since they are primarily designed to detect failed antennas. Other work considered arrays subject to random element defects, blockages and/or hardware glitches, and proposed CS techniques to estimate the effective channel [21]-[23]. Effective channel estimates maximize the receiver (or transmitter) gain and does not provide information related to the location of the failed or blocked antennas. This information allows the receiver (or transmitter) to optimize its beam pattern in order to maximize its gain or minimize its sidelobe level.

In this paper, we first study the effects of random blockages on the far-field radiation pattern of a linear uniform

antenna array. We consider partial and complete blockages, and show that both types of blockages randomize the far-field radiation pattern of the array. This randomization causes uncertainty in the mmWave channel. We then present closed-form expressions for the mean and variance of the far-field radiation pattern as a function of the antenna element blockage probability. These expressions provide an efficient means to evaluate the impact of the number of antenna elements and the antenna element blockage probability on the far-field radiation pattern and the effective mmWave channel.

To detect blockages, we propose two CS based array diagnosis techniques for mmWave antenna arrays. The proposed techniques are different from the CS diagnosis techniques proposed in [19] and [20] since those techniques: (i) detect the sparsity pattern of a failed array and not necessary blockages, (ii) require measurements to be made at multiple locations, (iii) assume error-free samples, i.e. faults at the AUT only, and (iv) do not estimate the effective antenna element gains, i.e. the induced attenuation and phase shifts caused by blockages. The proposed CS techniques take into account these limitations and permit array diagnosis with reduced number of measurements. The first technique detects blockages at the receiver's array and assumes a fault free array at the transmitter, while the second technique detects blockages at both the transmit and receive arrays. When blockages exist at the receiver, the receiver requests a transmitter to transmit  $K$  training symbols. As shown in Fig. 2(a), the receiver receives each training symbol using a random beam. Using CS, we will show that the proposed techniques estimate (i) fault locations, i.e. the locations of the particles suspended on the antenna array, and (ii) the attenuation and phase shifts caused by these particles. When blockages exist at both the transmit and receive arrays, the transmitter forms  $K$  random beams and uses each beam to transmit a training symbol to the receiver. The receiver receives each symbol using a random receive beam as shown in Fig. 2(b). The random beams are required to randomly sample the arrays under test. We show that by using CS techniques, the receiver jointly estimates the fault locations and the attenuation and phase shifts caused by blockages at both the transmit and receive arrays.

The remainder of this paper is organized as follows. In Section II, we formulate the array diagnosis problem. In Section III, we study the effects of random blockages on the far-field radiation pattern of linear arrays. In Section IV, we introduce the proposed array diagnosis technique assuming a fault free transmit array and in Section V, we introduce the proposed array diagnosis technique when faults are present at both the transmit and receive arrays. In Section VI we provide some numerical results and conclude our work in Section VII.

## II. PROBLEM FORMULATION

We consider a two-dimensional (2D) planar antenna array with  $N_x$  equally spaced isotropic elements along the x-axis and  $N_y$  equally spaced isotropic elements along the y-axis; nonetheless, the model and the corresponding algorithms can be adapted to other antenna structures as well. Each antenna element is described by its positions along the x and y axis, for

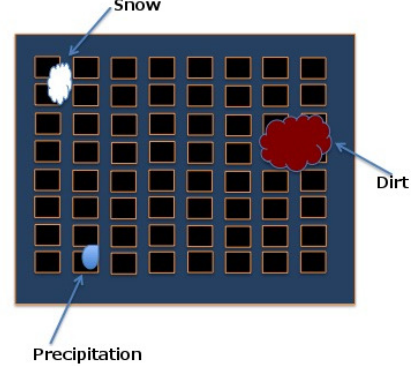


**Fig. 1:** An example of an outdoor millimeter wave antenna array with different suspended particles partially blocking the array. The suspended particles, with different absorption and scattering properties, modify the array geometry.

example, the  $(n_x, n_y)$ th antenna refers to an antenna located at the  $n_x$ th position along the x-axis and the  $n_y$ th position along the y-axis. The ideal far-field radiation pattern of this planar array in the direction  $(\theta, \phi)$  is given by [24]

$$f(\theta, \phi) = \sum_{n=0}^{N_y-1} \sum_{m=0}^{N_x-1} w_{n,m} e^{jm \frac{2\pi d_x}{\lambda} \sin \theta \cos \phi} e^{jn \frac{2\pi d_y}{\lambda} \sin \theta \sin \phi}, \quad (1)$$

where  $d_x$  and  $d_y$  are the antenna spacing along the x and y axis,  $\lambda$  is the wavelength, and  $w_{n,m}$  is the  $(n, m)$ th complex antenna weight.

Let  $\mathbf{a}_x(\theta, \phi) \in \mathcal{C}^{N_x \times 1}$  and  $\mathbf{a}_y(\theta, \phi) \in \mathcal{C}^{N_y \times 1}$  be two vectors where the  $m$ th entry of  $\mathbf{a}_x(\theta, \phi)$  is  $[\mathbf{a}_x(\theta, \phi)]_m = e^{jm \frac{2\pi d_x}{\lambda} \sin \theta \cos \phi}$  and the  $n$ th entry of  $\mathbf{a}_y(\theta, \phi)$  is  $[\mathbf{a}_y(\theta, \phi)]_n = e^{jn \frac{2\pi d_y}{\lambda} \sin \theta \sin \phi}$ . Also, let the matrix  $\mathbf{W} \in \mathcal{C}^{N_y \times N_x}$  be a matrix of antenna weights, where the  $(n, m)$ th entry of  $\mathbf{W}$  is  $[\mathbf{W}]_{n,m} = w_{n,m}$ . Then (1) can be reduced to

$$f(\theta, \phi) = \text{vec}(\mathbf{W})^T \mathbf{a}(\theta, \phi), \quad (2)$$

where  $\text{vec}(\mathbf{W})$  is the  $N_x N_y \times 1$  column vector obtained by stacking the columns of the matrix  $\mathbf{W}$  on top of one another, the vector  $\mathbf{a}(\theta, \phi) = \mathbf{a}_x(\theta, \phi) \otimes \mathbf{a}_y(\theta, \phi)$  is the 1D array response vector, and the operator  $\otimes$  represents the Kronecker product. The formulation in (2) allows us to represent the 2D array as a 1D array, and as a result, simplify the problem formulation.

In the presence blockages, the far-field radiation pattern of the array in (2) becomes

$$g(\theta, \phi) = \underbrace{\text{vec}(\mathbf{W})^T}_{\mathbf{x}} \underbrace{(\mathbf{b} \circ \mathbf{a}(\theta, \phi))}_{\mathbf{z}}, \quad (3)$$

where operator  $\circ$  represents the Hadamard product, and the vector  $\mathbf{b} \in \mathcal{C}^{N_x N_y \times 1}$  is a vector of complex coefficients that result from the absorption and scattering caused by the particles suspended on the antenna array [3]. In (3), the vector  $\mathbf{x} \in \mathcal{C}^{N_x N_y \times 1}$  is a vector of antenna weights and the vector  $\mathbf{z} \in \mathcal{C}^{N_x N_y \times 1}$  is the equivalent array response vector. The  $n$ th entry of the vector  $\mathbf{b}$  is defined by

$$b_n = \begin{cases} \kappa_n e^{j\Phi_n}, & \text{if the } n\text{th antenna is blocked} \\ 1, & \text{otherwise,} \end{cases} \quad (4)$$

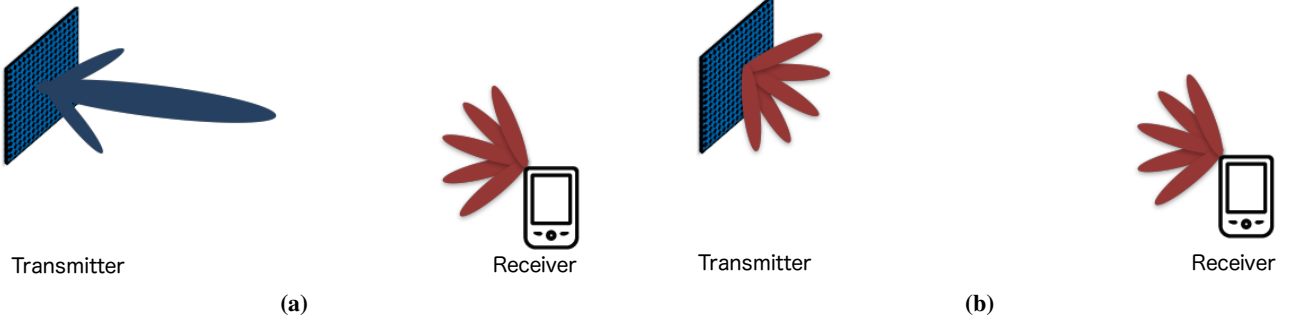


**Fig. 2:** Real time array diagnosis. (a) Diagnosis of the receiver array. Transmitter transmits  $K$  training symbols and the receiver receives each training symbol using a random receive beam. (b) Joint diagnosis of both the transmit and the receive arrays. Transmitter transmits  $K$  training symbols using random transmit beams and the receiver receives each training symbol using a random receive beam.

where  $n = 1, \dots, N_x N_y$ ,  $0 \leq \kappa_n \leq 1$  and  $0 \leq \Phi_n \leq 2\pi$  are the resulting absorption and scattering coefficients. A value of  $\kappa_n = 0$  represents maximum absorption (or blockage) at the  $n$ th antenna, and the scattering coefficient  $\Phi_n$  measures the phase-shift caused by the particle suspended on the  $n$ th antenna. It is clear from (3) that blockages will change the array manifold and result in a distorted radiation pattern as shown in Fig. 3. The resulting pattern is a function of the number of the particles suspended on the array and their corresponding dielectric constants. In the following, we first study the effects of blockages on the far-field radiation pattern of a linear array. Following that, we propose compressed sensing techniques that simultaneously estimate the locations of the blocked antennas and the corresponding attenuation and phase shifts caused by the suspended particles. Based on the estimated values of the vector  $\mathbf{b}$ , pattern correction techniques, see e.g. [8]-[13], can be employed to recalculate the excitation weights and, as a result, minimize the effects of blockages.

### III. EFFECTS OF BLOCKAGES ON THE FAR-FIELD BEAM PATTERN

In this section, we study the effects of blockages on the far-field radiation pattern of a linear antenna array. For ease of exposition, we study the effect of blockages on the azimuth direction only. A similar analysis can be performed for the elevation pattern.

From (3), the radiation pattern of an antenna array with  $N$  equally spaced elements along the  $x$ -axis with possible blockages can be written as

$$g(\phi) = \sum_{n=0}^{N-1} w_n b_n e^{jn \frac{2\pi d_x}{\lambda} \cos(\phi)}. \quad (5)$$

It is clear from (5) that random blockages distort the array manifold and result in a distorted beam pattern. Let  $\mathcal{I}_k$  be a set of  $S$  blocked antennas, and  $\mathcal{I}_n$  be a set of  $N - S$  fault-free antennas. Due to random blockages, the indices in both sets are random. If the AUT is steered towards  $\phi = \phi_T$ , the  $n$ th weight is set as  $w_n = e^{-jn \frac{2\pi d_x}{\lambda} \cos(\phi_T)}$ , and the normalized

amplitude at  $\phi = \phi_T$  becomes

$$\begin{aligned} g(\phi_T) &= \frac{1}{N} \sum_{n \in \mathcal{I}_n} e^{-jn \frac{2\pi d_x}{\lambda} \cos(\phi_T)} e^{jn \frac{2\pi d_x}{\lambda} \cos(\phi_T)} + \\ &\quad \frac{1}{N} \sum_{n \in \mathcal{I}_k} b_n e^{-jn \frac{2\pi d_x}{\lambda} \cos(\phi_T)} e^{jn \frac{2\pi d_x}{\lambda} \cos(\phi_T)} \quad (6) \end{aligned}$$

$$= \frac{N - S}{N} + \frac{Sb}{N} = 1 - \frac{S(1 - b)}{N}, \quad (7)$$

and the amplitude at  $\phi \neq \phi_T$  becomes

$$\begin{aligned} g(\phi) &= \frac{1}{N} \sum_{n \in \mathcal{I}_n} e^{jn \frac{2\pi d_x}{\lambda} (\cos(\phi) - \cos(\phi_T))} + \\ &\quad \frac{1}{N} \sum_{n \in \mathcal{I}_k} b_n e^{jn \frac{2\pi d_x}{\lambda} (\cos(\phi) - \cos(\phi_T))}. \quad (8) \end{aligned}$$

From (7) and (8) we observe that if  $b_{n \in \mathcal{I}_k} = 1$ , i.e. no blockages, the normalized amplitude of both the mainlobe and sidelobe is constant, however, if  $b_{n \in \mathcal{I}_k} \neq 1$ , there is a loss in the normalized amplitude of the main lobe, and the sidelobe amplitude becomes a random variable that is dependent on the location and intensity of the blockages. To study the effect of blockages, we derive the mean and variance of the far-field beam pattern. We undertake this study in the following sections.

#### A. Effect of blockages on the main lobe of the far-field beam pattern

1) *Constant Blockages:* In this section we consider constant blockages and study their effect on the main lobe. Let  $\forall n, b_n = b$  and the random variable  $B_n = b$  with probability  $P_b$ , and  $B_n = 1$  with probability  $1 - P_b$ . The term  $P_b = \frac{S}{N}$  represents the  $n$ th antenna blockage probability.

The mean of the far-field beam pattern at  $\phi = \phi_T$  can then be derived as

$$\mathbb{E}[g(\phi)] = \mathbb{E}\left[\frac{1}{N} \sum_{n=0}^{N-1} B_n e^{jn \frac{2\pi d_x}{\lambda} (\cos(\phi_T) - \cos(\phi_T))}\right] = \mathbb{E}[B_n],$$

where  $\mathbb{E}[B_n] = \Pr(B_n = 1)(1) + \Pr(B_n \neq 1)(b) = 1 - P_b + P_b b$ .

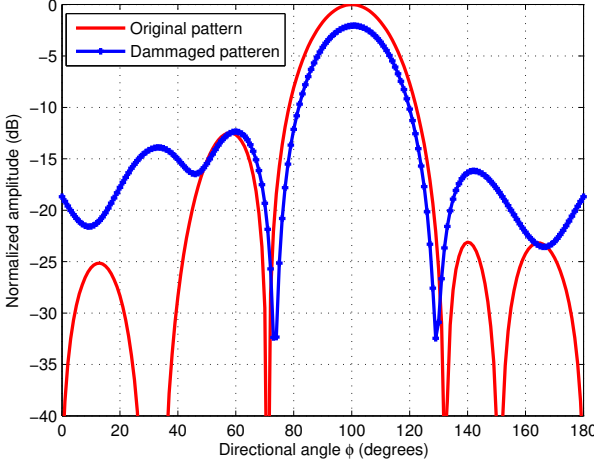


**Fig. 3:** Original and damaged beam patterns of a 16 element ( $4 \times 4$ ) planar array with  $\theta = 90$  degrees and  $\frac{d_x}{\lambda} = \frac{d_y}{\lambda} = 0.5$ . The third, fifth and seventh array elements of the equivalent 1D array (see (2)) are blocked with  $b_3 = 0.37 + j0.22$ ,  $b_5 = -0.1 + j0.34$ , and  $b_7 = -0.64 - j0.1$ . Blockages result in an increase in the sidelobe level and a decrease in gain.

Similarly, the variance of the far-field beam pattern at  $\phi = \phi_T$  can be derived as

$$\text{var}[g(\phi)] = \text{var} \left[ \frac{1}{N} \sum_{n \in \mathcal{I}_n} e^{jn \frac{2\pi d_x}{\lambda} (\cos(\phi_T) - \cos(\phi))} + \frac{1}{N} \sum_{n \in \mathcal{I}_k} b_n e^{jn \frac{2\pi d_x}{\lambda} (\cos(\phi_T) - \cos(\phi))} \right] \quad (9)$$

$$= 0 + \text{var} \left[ \frac{1}{N} \sum_{n \in \mathcal{I}_k} b_n e^{jn \frac{2\pi d_x}{\lambda} (\cos(\phi_T) - \cos(\phi))} \right] \quad (10)$$

where the last equality results since the value of  $b$  is constant throughout the array.

2) *Random Blockages*: When the antenna array is subject to random blockages, each antenna experiences random absorption and scattering. The mean of the far-field beam pattern at  $\phi = \phi_T$  can be derived as

$$\mathbb{E}[g(\phi)] = \mathbb{E} \left[ \frac{1}{N} \sum_{n \in \mathcal{I}_n} e^{jn \frac{2\pi d_x}{\lambda} (\cos(\phi_T) - \cos(\phi))} + \frac{1}{N} \sum_{n \in \mathcal{I}_k} b_n e^{jn \frac{2\pi d_x}{\lambda} (\cos(\phi_T) - \cos(\phi))} \right] \quad (11)$$

$$= \frac{N-S}{N} + \mathbb{E} \left[ \frac{1}{N} \sum_{n \in \mathcal{I}_k} b_n e^{jn \frac{2\pi d_x}{\lambda} (\cos(\phi_T) - \cos(\phi))} \right] \quad (12)$$

where the value of  $\mathbb{E}[b_n]$  depends on the distribution of the attenuation caused by the blocking particles, i.e. the distribution of  $b_n$ .

Similarly, the variance of the far-field beam pattern at  $\phi =$

$\phi_T$  can be derived as

$$\begin{aligned} \text{var}[g(\phi)] &= \text{var} \left[ \frac{1}{N} \sum_{n \in \mathcal{I}_n} e^{jn \frac{2\pi d_x}{\lambda} (\cos(\phi_T) - \cos(\phi))} + \frac{1}{N} \sum_{n \in \mathcal{I}_k} b_n e^{jn \frac{2\pi d_x}{\lambda} (\cos(\phi_T) - \cos(\phi))} \right] \\ &= \text{var} \left[ \frac{1}{N} \sum_{n \in \mathcal{I}_n} e^{jn \frac{2\pi d_x}{\lambda} (\cos(\phi_T) - \cos(\phi))} \right] + \text{var} \left[ \frac{1}{N} \sum_{n \in \mathcal{I}_k} b_n e^{jn \frac{2\pi d_x}{\lambda} (\cos(\phi_T) - \cos(\phi))} \right] \\ &= 0 + \text{var} \left[ \frac{1}{N} \sum_{n \in \mathcal{I}_k} b_n e^{jn \frac{2\pi d_x}{\lambda} (\cos(\phi_T) - \cos(\phi))} \right] \\ &= \text{var}[b_n] \left( \frac{S}{N} \right)^2 = \text{var}[b_n] P_b^2, \end{aligned} \quad (13)$$

where the term  $\text{var}[b_n]$  depends on the distribution of  $b_n$ .

### B. Effects of blockages on the sidelobes of the far-field beam pattern

1) *Constant Blockages*: The mean of the far-field beam pattern at  $\phi \neq \phi_T$  with constant blockages can be derived as

$$\mathbb{E}[g(\phi)] = \mathbb{E} \left[ \frac{1}{N} \sum_{n=0}^{N-1} B_n e^{jn \frac{2\pi d_x}{\lambda} (\cos(\phi) - \cos(\phi_T))} \right] \quad (14)$$

$$= \mathbb{E}[B_n] \left[ \frac{1}{N} \sum_{n=0}^{N-1} e^{jn \frac{2\pi d_x}{\lambda} (\cos(\phi) - \cos(\phi_T))} \right] \quad (15)$$

$$\begin{aligned} &= \left( \frac{N-S}{N^2} + \frac{Sb}{N^2} \right) \frac{1 - e^{jN \frac{2\pi d_x}{\lambda} (\cos(\phi) - \cos(\phi_T))}}{1 - e^{j \frac{2\pi d_x}{\lambda} (\cos(\phi) - \cos(\phi_T))}} \\ &= \left( \frac{1 - P_b(1-b)}{N} \right) \frac{\sin(N \frac{\pi d_x}{\lambda} (\cos(\phi) - \cos(\phi_T)))}{\sin(\frac{\pi d_x}{\lambda} (\cos(\phi) - \cos(\phi_T)))} \times \\ &\quad e^{j(N-1) \frac{\pi d_x}{\lambda} (\cos(\phi) - \cos(\phi_T))}. \end{aligned} \quad (16)$$

To derive the variance of  $g(\phi)$ , we decompose  $g(\phi)$  into its real and imaginary parts as follows

$$\begin{aligned} \text{var}[g(\phi)] &= \text{var}[\Re[g(\phi)]] + \text{var}[\Im[g(\phi)]] \\ &= \text{var} \left[ \Re \left[ \frac{1}{N} \sum_{n=0}^{N-1} B_n e^{jn \frac{2\pi d_x}{\lambda} (\cos(\phi) - \cos(\phi_T))} \right] \right] + \\ &\quad \text{var} \left[ \Im \left[ \frac{1}{N} \sum_{n=0}^{N-1} B_n e^{jn \frac{2\pi d_x}{\lambda} (\cos(\phi) - \cos(\phi_T))} \right] \right]. \end{aligned}$$

The variance of the real component can be expressed as

$$\begin{aligned} \text{var}[\Re[g(\phi)]] &= \text{var} \left[ \frac{1}{N} \sum_{n=0}^{N-1} B_n \cos \left( n \frac{2\pi d_x}{\lambda} (\cos(\phi) - \cos(\phi_T)) \right) \right] \\ &= \frac{\text{var}[B_n]}{N^2} \sum_{n=0}^{N-1} \cos^2 \left( n \frac{2\pi d_x}{\lambda} (\cos(\phi) - \cos(\phi_T)) \right). \end{aligned}$$

Similarly, the variance of the imaginary component can be expressed as

$$\begin{aligned} \text{var}[\Im[g(\phi)]] &= \text{var}\left[\frac{1}{N} \sum_{n=0}^{N-1} B_n \sin\left(n \frac{2\pi d_x}{\lambda} (\cos(\phi) - \cos(\phi_T))\right)\right] \\ &= \frac{\text{var}[B_n]}{N^2} \sum_{n=0}^{N-1} \sin^2\left(\cos\left(n \frac{2\pi d_x}{\lambda} (\cos(\phi) - \cos(\phi_T))\right)\right). \end{aligned}$$

Adding  $\text{var}[\Re[g(\phi)]]$  and  $\text{var}[\Im[g(\phi)]]$  we obtain

$$\begin{aligned} \text{var}[g(\phi)] &= \text{var}[B_n] \sum_{n=0}^{N-1} \cos^2\left(\cos\left(n \frac{2\pi d_x}{\lambda} (\cos(\phi) - \cos(\phi_T))\right)\right) + \\ &\quad \sin^2\left(\cos\left(n \frac{2\pi d_x}{\lambda} (\cos(\phi) - \cos(\phi_T))\right)\right) = \frac{\text{var}[B_n]}{N}, \end{aligned}$$

where the variance  $\text{var}[B_n]$  can be derived as

$$\begin{aligned} \text{var}[B_n] &= \mathbb{E}[B_n^2] - (\mathbb{E}[B_n])^2 = \Pr(B_n = 1)(1)^2 + \\ &\quad \Pr(B_n \neq 1)(|b|)^2 - (\mathbb{E}[B_n])^2 \\ &= \frac{N-S}{N} + \frac{S|b|^2}{N} - \left(\frac{N-S}{N} + \frac{Sb}{N}\right)^2. \end{aligned} \quad (17)$$

2) *Random Blockages*: To derive the mean and variance in this case, let the random variable  $c_n = 1$  with probability  $P_b$  if the the  $n$ th antenna is blocked and zero otherwise. The mean of the far-field beam pattern at  $\phi \neq \phi_T$  with random blockages becomes

$$\begin{aligned} \mathbb{E}[g(\phi)] &= \mathbb{E}\left[\frac{1}{N} \sum_{n=0}^{N-1} (1 - c_n) e^{jn \frac{2\pi d_x}{\lambda} (\cos(\phi) - \cos(\phi_T))}\right] + \\ &\quad \mathbb{E}\left[\frac{1}{N} \sum_{n=0}^{N-1} c_n b_n e^{jn \frac{2\pi d_x}{\lambda} (\cos(\phi) - \cos(\phi_T))}\right] \\ &= \mathbb{E}[(1 - c_n)] \left[ \frac{1}{N} \sum_{n=0}^{N-1} e^{jn \frac{2\pi d_x}{\lambda} (\cos(\phi) - \cos(\phi_T))} \right] + \\ &\quad \mathbb{E}[c_n b_n] \left[ \frac{1}{N} \sum_{n=0}^{N-1} e^{jn \frac{2\pi d_x}{\lambda} (\cos(\phi) - \cos(\phi_T))} \right] \\ &= \frac{\mathbb{E}[(1 - c_n)] + \mathbb{E}[c_n b_n]}{N} \sum_{n=0}^{N-1} e^{jn \frac{2\pi d_x}{\lambda} (\cos(\phi) - \cos(\phi_T))} \\ &= \frac{\mathbb{E}[(1 - c_n)] + \mathbb{E}[c_n] \mathbb{E}[b_n]}{N} \frac{1 - e^{jN \frac{2\pi d_x}{\lambda} (\cos(\phi) - \cos(\phi_T))}}{1 - e^{j \frac{2\pi d_x}{\lambda} (\cos(\phi) - \cos(\phi_T))}} \\ &= \frac{1 - P_b(1 - \mathbb{E}[b_n])}{N} \frac{\sin(N \frac{\pi d_x}{\lambda} (\cos(\phi) - \cos(\phi_T)))}{\sin(\frac{\pi d_x}{\lambda} (\cos(\phi) - \cos(\phi_T)))} \times \\ &\quad e^{j(N-1) \frac{\pi d_x}{\lambda} (\cos(\phi) - \cos(\phi_T))}, \end{aligned}$$

where in (18)  $\mathbb{E}[(c_n)] = P_b$  and  $\mathbb{E}[(1 - c_n)] = 1 - P_b$ .

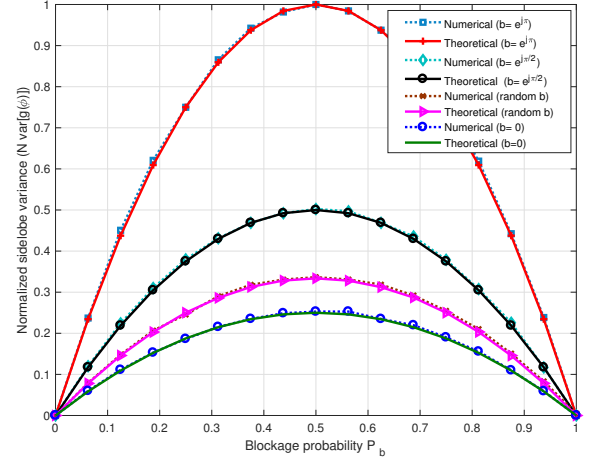


**Fig. 4:** Numerical and theoretical (eq. (17)) values of the sidelobe variance versus the number of blockages;  $N = 64$ , and  $\phi_T = 100^\circ$ .

Following (17), the variance of  $g(\phi)$  can be derived as

$$\begin{aligned} \text{var}[g(\phi)] &= \text{var}\left[\frac{1}{N} \sum_{n=0}^{N-1} (1 - c_n) e^{jn \frac{2\pi d_x}{\lambda} (\cos(\phi) - \cos(\phi_T))}\right] + \\ &\quad \text{var}\left[\frac{1}{N} \sum_{n=0}^{N-1} c_n b_n e^{jn \frac{2\pi d_x}{\lambda} (\cos(\phi) - \cos(\phi_T))}\right] \\ &= \frac{\text{var}[(1 - c_n)]}{N} + \frac{\text{var}[(c_n)] \text{var}[(b_n)]}{N}, \end{aligned} \quad (18)$$

where the variance  $\text{var}[c_n] = \mathbb{E}[c_n^2] - (\mathbb{E}[c_n])^2 = \Pr(c_n = 1)(1)^2 + \Pr(c_n = 0)(0) - (\mathbb{E}[c_n])^2 = P_b - P_b^2$ , and  $\text{var}[c_n] = \text{var}[1 - c_n]$ . Substituting  $\text{var}[1 - c_n]$  and  $\text{var}[c_n]$  in (18) we obtain

$$\text{var}[g(\phi)] = \frac{1}{N} \left( P_b - P_b^2 + (P_b - P_b^2) \text{var}[(b_n)] \right). \quad (19)$$

Tables I and II summarize the effects of blockages on the far-field beam pattern of a linear array. From Table I, we observe that both complete and partial blockages reduce the amplitude of the main lobe. This reduces the beamforming gain of the array. Interestingly, Table I shows that complete blockages have no effect on the variance of the of the main lobe, and hence do not cause any randomness in the main lobe. Partial blockages, however, randomize the main lobe and cause uncertainties in the mmWave channel. From Table II, we observe that complete and partial blockages distort the sidelobes of the far-field radiation pattern. Table II also shows that the variance of this distortion is a function of the blockage intensity, i.e., value of  $b$ , and the blockage probability  $P_b$ .

To gain insight on the effects of constant blockages on the sidelobes, we plot the beam pattern sidelobe variance versus the number of blockages for different values of blockage coefficients  $b$  in Fig. 4. For all cases, the figure shows that the sidelobe variance increases with the blockage probability  $P_b$ , plateaus, and then decreases. As  $P_b$  increases, most of the antenna elements become blocked. This reduces the randomness of the array geometry and results in a lower variance as shown in Fig. 4. Fig. 4 also shows that complete blockages ( $b = 0$ ) result in the minimum variance while partial blockages

**TABLE I:** Mean and variance of the far-field beam pattern of a linear array at  $\phi = \phi_T$  as a function of the antenna element blockage probability  $P_b$  and the blockage coefficient  $b$ . The blockage coefficient is constant if the array is subject to a single type of blockage, and variable if the array is subject to multiple types of blockages.

Fault Type	Mean	Variance
Complete blockage ( $b = 0$ )	$1 - P_b$	0
Partial blockage (constant $b$ )	$1 - P_b + P_b b$	0
Partial blockages (variable $b$ )	$1 - P_b + P_b \mathbb{E}[b]$	$P_b^2 \text{var}[b]$

**TABLE II:** Mean and variance of the far-field beam pattern of a linear array at  $\phi \neq \phi_T$  as a function of the antenna element blockage probability  $P_b$  and the blockage coefficient  $b$ ;  $\gamma = \frac{\pi d_x}{\lambda}(\cos(\phi) - \cos(\phi_T))$ .

Fault Type	Mean	Variance
Complete blockage	$(1 - P_b) \frac{\sin(N\gamma)}{N \sin(\gamma)} e^{j(N-1)\gamma}$	$\frac{P_b}{N} (1 - P_b)$
Partial blockage (constant $b$ )	$(1 - P_b(1-b)) \frac{\sin(N\gamma)}{N \sin(\gamma)} e^{j(N-1)\gamma}$	$\frac{1}{N} (1 - P_b + P_b b^2) - \frac{1}{N} (1 - P_b + P_b b)^2$
Partial blockage (variable $b$ )	$(1 - P_b(1 - \mathbb{E}[b])) \frac{\sin(N\gamma)}{N \sin(\gamma)} e^{j(N-1)\gamma}$	$\frac{P_b}{N} (1 - P_b)(1 + \text{var}[b])$

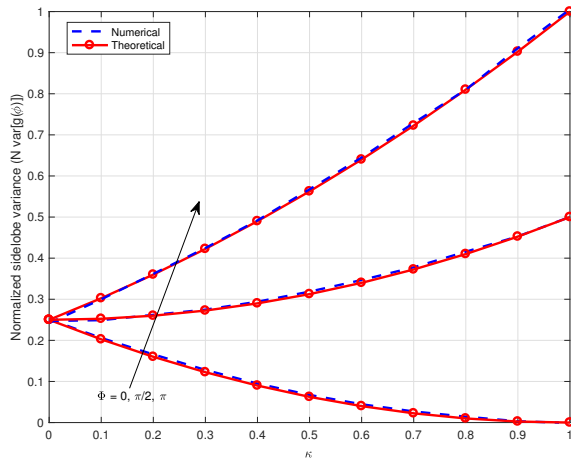


**Fig. 5:** Numerical and theoretical (eq. (17)) values of the normalized sidelobe variance versus the attenuation coefficient  $\kappa$ ;  $N = 64$ ,  $P_b = 0.5$ , and  $\phi_T = 100^\circ$ .

result in higher variance. Moreover, Fig. 4 shows that the theoretical value of the sidelobe variance is identical to the sidelobe variance obtained by Monte Carlo simulations. This verifies the correctness of our analysis and enables us to gain further insights into the impact of key parameters such as, the number of antenna elements and the blockage probability, on the sidelobe level variance.

In Fig. 5, we study the effect of partial and complete blockages on the sidelobe variance. The figure shows that the sidelobe variance decreases with higher values of  $\kappa$  (lower absorption intensity) when the blocking particles do not induce any phase shifts. When the blocking particles induce a phase shift, the figure shows that the variance increases with higher values of  $\kappa$ . Irrespective of the phase shift, the figure shows that complete blockages ( $\kappa = 0$ ) result in the minimum variance.

#### IV. FAULT DETECTION AT THE RECEIVER

In the previous section, we showed that blockages distort the beam pattern of the array, and as a result, cause uncertainties in the mmWave communication link. To mitigate the effects of blockages, it is imperative to design reliable array diagnosis techniques that detect the fault locations and estimate the

values of the blockage coefficients with minimum diagnosis time. In this section we propose an array diagnosis technique that detects blockages at the receive antenna array. It is assumed that the number of blocked antennas  $S \ll N_R$  and  $N_R = N_x N_y$  is large. The proposed technique can also be employed for a high number of blocked antennas, however, this comes at the expense of an increased detection time.

To detect blockages, the receiver with the AUT requests a transmitter, with known location, i.e.  $\theta$  and  $\phi$ , to transmit  $K$  training symbols (assumed to be known to the receiver). The receiver with the AUT generates a random beam to receive each training symbol as shown in Fig. 2(a), i.e., random antenna weights are used at the AUT to combine each training symbol. Mathematically, the  $k$ th output of the AUT can be written as

$$h_k(\theta, \phi) = \sqrt{\rho} s \mathbf{x}_k^T \mathbf{z} + e_k, \quad (20)$$

where  $k = 1, \dots, K$ ,  $\rho$  is the effective signal-to-noise ratio (SNR) which includes the path loss,  $s = 1$  is the training symbol, and  $e_k \sim \mathcal{CN}(0, 1)$  is the additive noise. The entries of the weighing vector  $\mathbf{x}_k$  at the  $k$ th instant are chosen uniformly and independently at random. Equipped with the path-loss and angular location of the transmitter, the receiver generates the ideal pattern  $f(\theta, \phi)$  using (1). Subtracting the ideal beam pattern from the received signal in (20) we obtain

$$y_k = h_k(\theta, \phi) - f_k(\theta, \phi) \quad (21)$$

$$= \mathbf{x}_k^T (\mathbf{b} \circ \mathbf{a}(\theta, \phi)) - \mathbf{x}_k^T \mathbf{a}(\theta, \phi) + \tilde{e}_k \quad (22)$$

$$= \mathbf{x}_k^T (\mathbf{c} \circ \mathbf{a}(\theta, \phi)) + \tilde{e}_k, \quad (23)$$

where  $\tilde{e}_k = \frac{e_k}{\sqrt{\rho}}$ , and the  $n$ th entry of the vector  $\mathbf{c}$  is  $\mathbf{c}(n) = 0$  when there is no blockage at the  $n$ th antenna, and  $\mathbf{c}(n) = b_n - 1$  otherwise. Let  $\mathbf{q} = \mathbf{c} \circ \mathbf{a}(\theta, \phi)$ , after  $K$  measurements we obtain

$$\begin{bmatrix} y_1 \\ y_2 \\ \vdots \\ y_K \end{bmatrix} = \underbrace{\begin{bmatrix} x_{1,1} & x_{1,2} & \cdots & x_{1,N_R} \\ x_{2,1} & x_{2,2} & \cdots & x_{2,N_R} \\ \vdots & \vdots & \ddots & \vdots \\ x_{K,1} & x_{K,2} & \cdots & x_{K,N_R} \end{bmatrix}}_{\mathbf{X}} \begin{bmatrix} q_1 \\ q_2 \\ \vdots \\ q_{N_R} \end{bmatrix} + \begin{bmatrix} \tilde{e}_1 \\ \tilde{e}_2 \\ \vdots \\ \tilde{e}_K \end{bmatrix}$$

or equivalently

$$\mathbf{y} = \mathbf{X}\mathbf{q} + \mathbf{e}. \quad (24)$$

Assuming that the number of blocked antenna elements is small, i.e.  $S \ll N_R$ , the vector  $\mathbf{q}$  in (24) becomes sparse with  $S$  non-zero elements that represent the locations of the blocked antennas.

To mitigate the effects of blockages, it is desired to first detect the locations of the blocked antennas and then the complex random variable  $b_n$  with few measurements (or diagnostic time). Note that the system in (24) requires  $K \geq N_R$  measurements to estimate the vector  $\mathbf{q}$ . While this might be acceptable for small antenna arrays, mmWave systems are usually equipped with large antenna arrays to provide sufficient link budget [26]. Scaling the number of measurements with the number of antennas would require more measurements and would increase the array diagnosis time. In the following, we show how we can (i) detect the locations of the blocked antennas, and (ii) estimate the complex blockage coefficients  $b_n$  with  $K \ll N_R$  measurements by exploiting the sparsity structure of the vector  $\mathbf{q}$ .

#### A. Blocked Antenna Detection Using the Least Absolute Shrinkage and Selection Operator

Compressive sensing theory permits efficient reconstruction of a sensed signal with only a few sensing measurements. While there are many different methods used to solve sparse approximation problems (see, e.g., [27], [28]), we employ the least absolute shrinkage and selection operator (LASSO) as a recovery method. We adopt the LASSO since it does not require the support of the vector  $\mathbf{q}$  to be known a priori. This makes it a suitable detection technique as blockages are random in general. The LASSO estimate of (24) is given by [27]

$$\arg \min_{\boldsymbol{\nu} \in \mathbb{C}^{N_R \times 1}} \frac{1}{2} \|\mathbf{y} - \mathbf{X}\boldsymbol{\nu}\|_{l_2}^2 + \alpha \sigma \|\boldsymbol{\nu}\|_{l_1}, \quad (25)$$

where  $\|\cdot\|_{l_1}$  and  $\|\cdot\|_{l_2}$  represent  $l_1$  and  $l_2$  norms, respectively,  $\sigma$  is the standard derivation of the noise  $\tilde{\mathbf{e}}$ , and  $\alpha$  is a regularization parameter.

It was shown in [27] that if the matrix  $\mathbf{X}$  satisfies the coherence property (i.e. the maximum cross correlation is bounded) and  $K > \Gamma S \log N_R$ , where  $\Gamma$  is a positive constant, the LASSO estimate identifies all non-zero entries of  $\mathbf{q}$  with probability  $\mathcal{P}_{\text{cs}} \geq 1 - \frac{2}{N_R} \left( \frac{1}{\sqrt{2\pi \log N_R}} + \frac{S}{N_R} \right)$  in the high SNR case [27]. Unlike the diagnostic techniques in [19] and [20], where the sensing matrices may not necessarily satisfy the coherence property, the matrix  $\mathbf{X}$  in (24) can be easily designed to satisfy the coherence property. For example, random IID Gaussian or Bernoulli matrices and partial Fourier or Walsh-Hadamard matrices are shown to satisfy the coherence property with high probability [25], [28], [29]. For simplicity, the antennas weights, i.e. the entries of the matrix  $\mathbf{X}$ , are randomly and uniformly selected from the set  $\{1 + j, 1 - j, -1 + j, -1 - j\}$  in this paper.

#### B. Attenuation and Induced Phase Shift Estimation

Once the support  $\mathcal{S}$ , where  $\mathcal{S} = \{n : q_n \neq 0\}$ , is estimated, one can apply estimation techniques such as least squares (LS) estimation to estimate the complex coefficient  $b_{n \in \mathcal{S}}$ . To achieve this, the columns of  $\mathbf{X}$  which are associated with the non-zero entries of  $\mathbf{q}$  are removed to obtain  $\mathbf{X}_{\mathcal{S}} \in \mathbb{C}^{K \times S}$ . Hence, the received vector  $\mathbf{y}$  in equation (24) can now be written as

$$\mathbf{y} = \mathbf{X}_{\mathcal{S}}\mathbf{q}_{\mathcal{S}} + \mathbf{e}, \quad (26)$$

where  $\mathbf{q}_{\mathcal{S}}$  is obtained from the vector  $\mathbf{q}$  by removing the entries associated with the non-zero value of  $\mathbf{q}$ . Since  $K > S$ , the entries of  $\mathbf{q}_{\mathcal{S}}$  can be estimated via LS estimation. In particular, one can write the LS estimate after successful sparsity pattern recovery as [30]

$$\hat{\mathbf{q}}_{\mathcal{S}} = (\mathbf{X}_{\mathcal{S}}^* \mathbf{X}_{\mathcal{S}})^{-1} \mathbf{X}_{\mathcal{S}}^* \mathbf{y} = \mathbf{q}_{\mathcal{S}} + \check{\mathbf{e}}, \quad (27)$$

where  $\hat{\mathbf{q}}_{\mathcal{S}}$  is a noisy estimate of  $\mathbf{q}_{\mathcal{S}}$ , and the entries of the output noise vector  $\check{\mathbf{e}}$  are Gaussian random variables as linear operations preserve the Gaussian noise distribution. Note that the  $n$ th entry of the vector  $\mathbf{q}$  is  $[\mathbf{q}]_n = (b_n - 1)a_n$ , where  $a_n$  is the  $n$ th entry of the vector  $\mathbf{a}(\theta, \phi)$  (see (21)-(24)). Therefore, the estimated attenuation coefficient  $\hat{\kappa}_{n \in \mathcal{S}} = |\frac{\hat{q}_{n \in \mathcal{S}}}{a_{n \in \mathcal{S}}} + 1|$  and the estimated induced phase  $\hat{\Phi}_{n \in \mathcal{S}} = \angle \left( \frac{\hat{q}_{n \in \mathcal{S}}}{a_{n \in \mathcal{S}}} + 1 \right)$ .

#### V. JOINT FAULT DETECTION AT THE TRANSMITTER AND THE RECEIVER

In the previous section, we assumed that the transmit antenna is free from blockages. When blockages exist at the transmit antenna, the receiver receives distorted training symbols and as a result, the technique proposed in the previous section will fail. In this section, we propose a detection technique that jointly detects blockages at both the transmitter and the receiver. For this technique, we assume that the receiver is equipped with the path-loss, angular location and array manifold of the transmitter. To start the diagnosis process, the transmitter transmits a training symbol  $s = 1$  using  $K$  random antenna weights (assumed to be known by the receiver). The receiver generates random antenna weights to receives each training symbol.

Let  $\mathbf{a}_T(\theta, \phi) = \mathbf{a}_{tx}(\theta, \phi) \otimes \mathbf{a}_{ty}(\theta, \phi)$  be the  $N_T \times 1$  1D transmit array response vector. The  $k$ th received measurement at the receiver becomes

$$y_k = \mathbf{w}_k^* (\mathbf{b} \circ \mathbf{a}(\theta, \phi)) (\mathbf{b}_T \circ \mathbf{a}_T(\theta, \phi))^* \mathbf{f}_k + \tilde{e}_k, \quad (28)$$

where  $\mathbf{b}_T$  is a vector of complex coefficients that result from the absorption and scattering caused by the particles blocking the transmit antenna array. After  $K$  measurements the receiver obtains the following measurement matrix

$$\mathbf{Y}_r = \mathbf{W}^* \mathbf{A} \mathbf{F} + \mathbf{E}, \quad (29)$$

where  $\mathbf{Y}_r = \text{diag}\{y_1, \dots, y_K\}$  is the received measurement matrix,  $\mathbf{W} \in \mathbb{C}^{N_R \times K}$  is a random weighting matrix at the receiver,  $\mathbf{A} = (\mathbf{b} \circ \mathbf{a}(\theta, \phi)) (\mathbf{b}_T \circ \mathbf{a}_T(\theta, \phi))^*$  is the  $N_R \times N_T$  equivalent array response matrix, the matrix  $\mathbf{F} \in \mathbb{C}^{N_T \times K}$  is a random weighting matrix at the transmitter, and  $\mathbf{E} =$

$\text{diag}\{\tilde{e}_1, \dots, \tilde{e}_K\}$  is the additive noise matrix. Equipped with the weighting matrices  $\mathbf{F}$  and  $\mathbf{W}$ , the receiver generates the ideal received vector  $\mathbf{Y}_I = \mathbf{W}^* \mathbf{A}_I \mathbf{F}$ , where  $\mathbf{A}_I = \mathbf{a}(\theta, \phi) \mathbf{a}_I^*(\theta, \phi)$ , and subtracts it from  $\mathbf{Y}_r$  in (29) to obtain

$$\mathbf{Y} = \mathbf{Y}_r - \mathbf{Y}_I = \mathbf{W}^* \mathbf{A}_s \mathbf{F} + \mathbf{E}, \quad (30)$$

where  $\mathbf{A}_s \in \mathbb{C}^{N_R \times N_T}$  is a sparse matrix. The non-zero entries of the columns of  $\mathbf{A}_s$  represent the indices of faulty antennas at the transmitter and the non-zero entries of the rows of  $\mathbf{A}_s$  represent the entries of the faulty antennas at the receiver. To formulate the CS recovery problem, we vectorize the measurement matrix  $\mathbf{Y}$  in (30) to obtain

$$\text{vec}(\mathbf{Y}) = \text{vec}(\mathbf{W}^* \mathbf{A}_s \mathbf{F}) + \text{vec}(\mathbf{E}) \quad (31)$$

$$= \underbrace{(\mathbf{W} \otimes \mathbf{F})}_{\mathbf{U}} \underbrace{\text{vec}(\mathbf{A}_s)}_{\mathbf{g}} + \underbrace{\text{vec}(\mathbf{E})}_{\mathbf{e}}, \quad (32)$$

where the matrix  $\mathbf{U}$  is the effective CS measurement matrix, and the vector  $\mathbf{g}$  is the effective sparse vector. Removing the  $K(K-1)$  zeros from the vector  $\mathbf{y} = \text{vec}(\mathbf{Y})$  we obtain

$$\bar{\mathbf{y}} = \bar{\mathbf{U}} \bar{\mathbf{g}} + \bar{\mathbf{e}}, \quad (33)$$

where  $\bar{\mathbf{y}} \in \mathbb{C}^{K \times 1}$ ,  $\bar{\mathbf{U}} \in \mathbb{C}^{K \times N_T N_R}$ ,  $\bar{\mathbf{g}} \in \mathbb{C}^{N_T N_R \times 1}$ , and  $\bar{\mathbf{e}} \in \mathbb{C}^{K \times 1}$ .

*Lemma 1:* Let  $\mathbf{A}$  and  $\mathbf{B}$  be two matrices with normalized columns and IID entries, and the matrix  $\mathbf{C} = \mathbf{A} \otimes \mathbf{B}$ . Denote the coherence of  $\mathbf{A}$  as  $\mu(\mathbf{A})$  and the coherence of  $\mathbf{B}$  as  $\mu(\mathbf{B})$ . The coherence of the matrix  $\mathbf{C}$  is  $\mu(\mathbf{C}) = \max(\mu(\mathbf{A}), \mu(\mathbf{B}))$ .

*Proof:* The coherence of  $\mathbf{C}$  is defined as the maximum absolute value of the cross-correlations between the columns of  $\mathbf{C}$  [31]

$$\mu(\mathbf{C}) = \max_{i \neq j} |\mathbf{c}_i^* \mathbf{c}_j|, \quad (34)$$

with  $\mathbf{c}_i$  and  $\mathbf{c}_j$  denoting the  $i$ th and  $j$ th columns of the matrix  $\mathbf{C}$ . Note that  $\mathbf{c}_i = \mathbf{a}_i \otimes \mathbf{b}_k$  and  $\mathbf{c}_j = \mathbf{a}_j \otimes \mathbf{b}_l$ . Substituting in (34) we obtain

$$\begin{aligned} \mu(\mathbf{C}) &\stackrel{(a)}{=} \max_{i \neq j, k \neq l} \left( |(\mathbf{a}_i \otimes \mathbf{b}_k)^* (\mathbf{a}_j \otimes \mathbf{b}_l)|, \right. \\ &\quad \left. |(\mathbf{a}_i \otimes \mathbf{b}_k)^* (\mathbf{a}_i \otimes \mathbf{b}_l)|, |(\mathbf{a}_i \otimes \mathbf{b}_k)^* (\mathbf{a}_j \otimes \mathbf{b}_k)| \right) \\ &\stackrel{(b)}{=} \max_{i \neq j, k \neq l} \left( |(\mathbf{a}_i^* \mathbf{a}_j)(\mathbf{b}_k^* \mathbf{b}_l)|, |(\mathbf{a}_i^* \mathbf{a}_j)(\mathbf{b}_k^* \mathbf{b}_k)|, \right. \\ &\quad \left. |(\mathbf{a}_i^* \mathbf{a}_i)(\mathbf{b}_k^* \mathbf{b}_l)| \right) \\ &= \max \left( \max_{i \neq j} |(\mathbf{a}_i^* \mathbf{a}_j)| \max_{k \neq l} |(\mathbf{b}_k^* \mathbf{b}_l)|, \max_{i \neq j} |(\mathbf{a}_i^* \mathbf{a}_j)|, \right. \\ &\quad \left. \max_{k \neq l} |(\mathbf{b}_k^* \mathbf{b}_l)| \right) \\ &= \max(\mu(\mathbf{A})\mu(\mathbf{B}), \mu(\mathbf{A}), \mu(\mathbf{B})) \\ &\stackrel{(c)}{=} \max(\mu(\mathbf{A}), \mu(\mathbf{B})), \end{aligned} \quad (35)$$

where (b) results by applying Lemma 4.2.10 in [32] to the Kronecker product in (a), and (c) results since  $\mu(\mathbf{A})\mu(\mathbf{B}) \leq \min(\mu(\mathbf{A}), \mu(\mathbf{B}))$ .  $\blacksquare$

From Lemma 1 we conclude that if the matrices  $\mathbf{W}$  and  $\mathbf{F}$  in (31) both satisfy the coherence property, examples include

Gaussian, Bernoulli and Fourier matrices [25], then the matrix  $\mathbf{U} = \mathbf{W} \otimes \mathbf{F}$  also satisfies the coherence property and it can be applied in standard CS techniques. For simplicity, the entries of  $\mathbf{W}$  and  $\mathbf{F}$  are chosen uniformly and independently at random from the set  $\{1+j, 1-j, -1+j, -1-j\}$  in this paper.

### A. Sparsity Pattern Detection and Least Squares Estimation

The LASSO estimate of (33) is given by

$$\arg \min_{\boldsymbol{\nu} \in \mathbb{C}^{N_T N_R \times 1}} \frac{1}{2} \|\bar{\mathbf{y}} - \bar{\mathbf{U}} \boldsymbol{\nu}\|_2^2 + \alpha \sigma_e \|\boldsymbol{\nu}\|_{l_1}, \quad (36)$$

where  $\sigma_e$  is the standard derivation of the noise  $\bar{e}$ , and  $\alpha$  is a regularization parameter. Once the support  $\mathcal{S}$ , where  $\mathcal{S} = \{i : \bar{g}_i \neq 0\}$ , of the vector  $\bar{\mathbf{g}}$  is estimated, the columns of  $\bar{\mathbf{U}}$  which are associated with the non-zero entries of  $\bar{\mathbf{g}}$  are removed to obtain  $\bar{\mathbf{U}}_{\mathcal{S}}$ . Hence, the received vector  $\bar{\mathbf{y}}$  in (33) becomes

$$\bar{\mathbf{y}} = \bar{\mathbf{U}}_{\mathcal{S}} \bar{\mathbf{g}}_{\mathcal{S}} + \bar{\mathbf{e}}, \quad (37)$$

where  $\bar{\mathbf{g}}_{\mathcal{S}}$  is obtained from the vector  $\bar{\mathbf{g}}$  by removing the entries associated with the non-zero values of  $\bar{\mathbf{g}}$ . The LS estimate after successful sparsity pattern recovery becomes

$$\hat{\mathbf{g}}_{\mathcal{S}} = (\bar{\mathbf{U}}_{\mathcal{S}}^* \bar{\mathbf{U}}_{\mathcal{S}})^{-1} \bar{\mathbf{U}}_{\mathcal{S}}^* \bar{\mathbf{y}} = \bar{\mathbf{g}}_{\mathcal{S}} + \bar{\mathbf{e}}, \quad (38)$$

where  $\hat{\mathbf{g}}_{\mathcal{S}}$  is a noisy estimate of  $\bar{\mathbf{g}}_{\mathcal{S}}$ .

### B. Attenuation and Induced Phase Shift Estimation

Let  $\mathbf{r}$  be a vector of size  $N_T N_R \times 1$  and its  $i$ th entry is given by

$$r_i = \begin{cases} \hat{g}_i & \text{in (38),} \\ 0 & \text{otherwise.} \end{cases} \quad (39)$$

Reshaping  $\mathbf{r}$  into  $N_R$  rows and  $N_T$  columns we obtain an estimate  $\hat{\mathbf{A}}_s$  of the sparse matrix  $\mathbf{A}_s$  in (30). The non-zero columns of  $\hat{\mathbf{A}}_s$  represent the IDs of the transmit array faulty antennas, and the non-zero rows of  $\hat{\mathbf{A}}_s$  represent the IDs of the receive array faulty antennas. Let the set  $\mathcal{I}_r$  contain the indices of the zero rows of  $\hat{\mathbf{A}}_s$  and the set  $\mathcal{I}_t$  contain the indices of the zero columns of  $\hat{\mathbf{A}}_s$ . Removing the rows associated with the IDs of the faulty receive antennas from  $\hat{\mathbf{A}}_s$  we obtain the matrix  $\mathbf{A}_r = [\hat{\mathbf{A}}_s]_{\mathcal{I}_r, :}$ , and the sparse vector that represents the faulty transmit antennas becomes

$$\hat{\mathbf{q}}_r = \frac{(\mathbf{a}_r(\theta, \phi)^* \mathbf{A}_r)^*}{\|\mathbf{a}_r(\theta, \phi)\|_2^2}, \quad (40)$$

where the vector  $\mathbf{a}_r(\theta, \phi)$  results from selecting the  $\mathcal{I}_r$  entries from the vector  $\mathbf{a}(\theta, \phi)$  in (28). Based on (40), the estimated attenuation coefficient and induced phase of the  $i$ th antenna element at the transmit array becomes  $\hat{\kappa}_{t,i} = |\frac{[\mathbf{q}_t]_i}{[\mathbf{a}_r(\theta, \phi)]_i} + 1|$  and  $\hat{\Phi}_{t,i} = \angle\left(\frac{[\mathbf{q}_t]_i}{[\mathbf{a}_r(\theta, \phi)]_i} + 1\right)$ .

Similarly, removing the columns associated with the IDs of the faulty antennas from  $\hat{\mathbf{A}}_s$  we obtain the matrix  $\mathbf{A}_t = [\hat{\mathbf{A}}_s]_{:, \mathcal{I}_t}$ , and the sparse vector that represents the faulty receive antennas becomes

$$\hat{\mathbf{q}}_t = \frac{\mathbf{A}_t \mathbf{a}_t(\theta, \phi)}{\|\mathbf{a}_t(\theta, \phi)\|_2^2}, \quad (41)$$

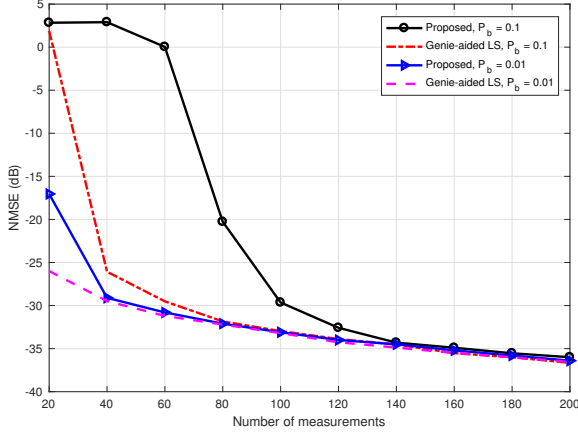


**Fig. 6:** Detection of faults in a 2D receive planar array subjected to random partial blockages with different blockage probability  $P_b$ ;  $\rho = 10$  dB, and  $N_R = 16 \times 16 = 256$ .

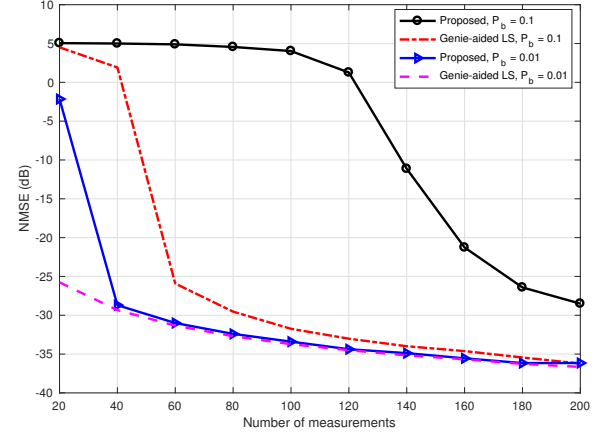


**Fig. 7:** Detection of faults in a 2D receive planar array subjected to random partial blockages with different blockage probability  $P_b$ ;  $\rho = 10$  dB, and  $N_R = 16 \times 32 = 512$ .

where the vector  $\mathbf{a}_t(\theta, \phi)$  results from selecting the  $\mathcal{I}_t$  entries from the vector  $\mathbf{a}_T(\theta, \phi)$  in (28). From (41), the estimated attenuation coefficient and induced phase of the  $i$ th antenna element at the receive array becomes  $\hat{\kappa}_{r,i} = \left| \frac{[\hat{\mathbf{q}}_r]_i}{[\mathbf{a}(\theta, \phi)]_i} + 1 \right|$  and  $\hat{\Phi}_{r,i} = \angle \left( \frac{[\hat{\mathbf{q}}_r]_i}{[\mathbf{a}(\theta, \phi)]_i} + 1 \right)$ .

## VI. NUMERICAL VALIDATION

In this section, we conduct numerical simulations to evaluate the performance of the proposed techniques. We consider two types of faults. The first type occurs when an antenna element is completely blocked and the second type occurs when an antenna element is partially blocked. A partial block can either result in a power reduction or simply induce a phase shift on an incident signal. For both cases, we assume a 2D planar array, with  $\frac{d_x}{\lambda} = \frac{d_y}{\lambda} = 0.5$ , that experiences random and independent blockages with probability  $P_b$ . To generate the random blockages, the values of  $\kappa$  and  $\Phi$  in (4) are chosen uniformly and independently at random from the set  $\{i \in \mathcal{R} : 0 \leq i \leq 1\}$  and  $\{0, \dots, 2\pi\}$  respectively. We adopt the success probability, i.e. the probability that all faulty antennas are detected, and the normalized mean square error (NMSE) as a performance measure to quantify the error in detecting the blocked antenna locations and estimating the corresponding blockage coefficients ( $\kappa$  and  $\Phi$ ). The NMSE is defined by

$$\text{NMSE} = \frac{\|\mathbf{v} - \hat{\mathbf{v}}\|_2^2}{\|\mathbf{v}\|_2^2}. \quad (42)$$

When blockages only exist at the receiver,  $\mathbf{v} = \mathbf{c} \circ \mathbf{a}(\theta, \phi)$  (see (23)), and the  $i$ th entry of the estimated vector  $\hat{\mathbf{v}}$  is  $[\hat{\mathbf{v}}]_{i \in \mathcal{S}} = [\hat{\mathbf{q}}]_{i \in \mathcal{S}}$  in (27) and zero otherwise. When blockages exist at both the receiver and the transmitter,  $\mathbf{v} = (\mathbf{b}_T \circ \mathbf{a}_T) - \mathbf{a}_T$  (see (28) and (30)) and  $\hat{\mathbf{v}} = \hat{\mathbf{q}}_t$  in (40) when detecting blockages at the transmitter array, and  $\mathbf{v} = (\mathbf{b} \circ \mathbf{a}) - \mathbf{a}$  and  $\hat{\mathbf{v}} = \hat{\mathbf{q}}_r$  in (41) when detecting blockages at the receiver array. To implement the LASSO, we use the function *SolveLasso* included in the *SparseLab* toolbox [33]. As a benchmark, we compare the NMSE of the proposed techniques with the

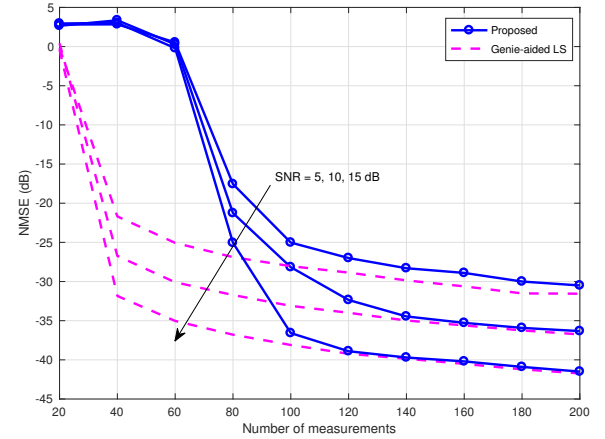


**Fig. 8:** Detection of faults in a 2D receive planar array subjected to random partial blockages with different receiver SNR;  $P_b = 0.1$ , and  $N_R = 16 \times 16 = 256$ .

NMSE of the Genie aided LS estimate which indicates the optimal estimation performance when the exact locations of the faulty antennas is known, i.e., the support  $\mathcal{S}$  in (27) and (38) is assumed to be provided by a Genie.

In Figs. 6-9 we consider faults at the receiver antenna array and assume that the transmitter antenna array is fault free. To study the effect of the number of measurements (or diagnosis time) on the performance of the proposed fault detection technique in Section IV, we plot the NMSE when the receive array is subject to blockages with different probabilities in Fig. 6. For all cases, we observe that the NMSE decreases with increasing number of measurements  $K$ . The figure also shows that for sufficient number of measurements (on the order of  $K \sim \mathcal{O}(P_b N_R \log N_R)$ ), the NMSE of the proposed technique matches the NMSE obtained by the Genie-aided LS technique. This indicates for sufficient number of measurements, the proposed technique successfully detects the locations of the blocked antennas and the corresponding blockage coefficients

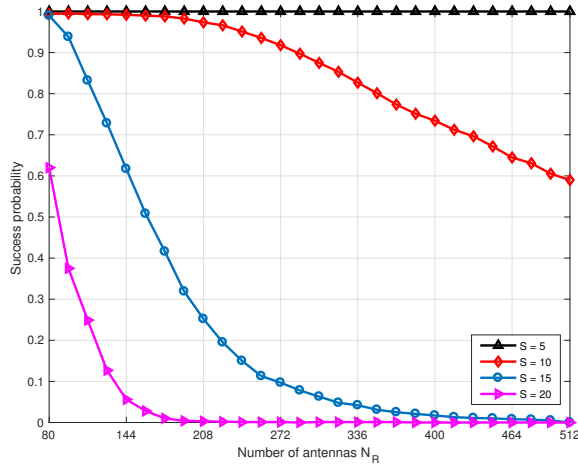


**Fig. 9:** Detection of faults in 2D receive planar arrays subject to complete blockages;  $\rho = 10$  dB,  $b_n \in \{0, 1\}$ , and the number of measurements is fixed to  $K = 45$ .

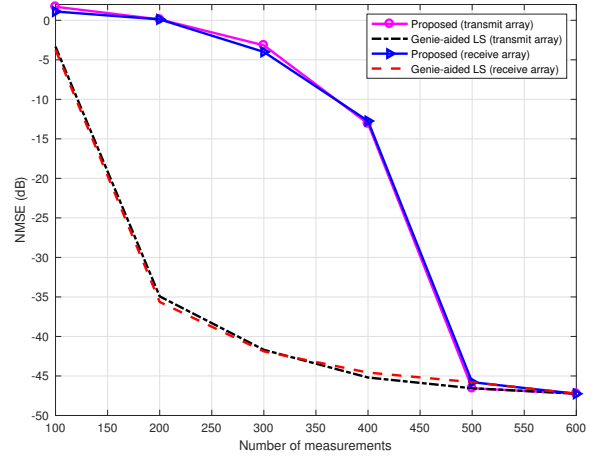


**Fig. 11:** Joint detection of faults in 2D transmit and receive planar arrays both subject to random partial blockages;  $P_b = 0.1$  for both arrays,  $\rho = 0$  dB,  $N_R = 32$ ,  $N_T = 32$ , and  $N_T N_R = 1024$ .

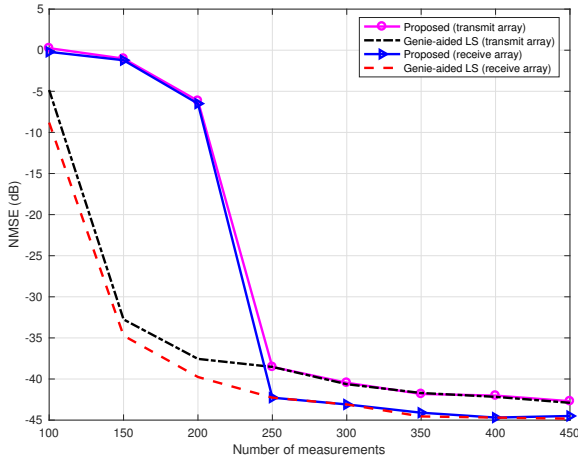


**Fig. 10:** Joint detection of faults in 2D transmit and receive planar arrays both subject to random partial blockages;  $P_b = 0.1$  for both arrays,  $\rho = 0$  dB,  $N_R = 16$ ,  $N_T = 32$ , and  $N_T N_R = 512$ .

with  $K \ll N_R$  measurements. The figure also shows that as the blockage probability increases, more measurements are required to reduce the NMSE. The reason for this is that as the blockage probability increases, the average number of blocked antennas increases as well. Therefore, more measurements are required to estimate the locations of the blocked antennas and the corresponding blockage coefficients.

To examine the effect of the array size on the number of measurements, we plot the NMSE of the proposed technique with  $N_R = 512$  in Fig. 7. The figure shows that the NMSE decreases with increasing number of measurements  $K$ . Nonetheless, this decrease occurs at a lower rate when compared to the case when  $N_R = 256$  in Fig. 6. This is particularly observed for higher blockage probabilities. The reason for this is that as the array size increases, the average number of blocked antennas increases as well. Therefore, more

measurements are required to estimate the locations of the blocked antennas and the corresponding blockage coefficients.

The effect of the SNR on the performance of the proposed technique is shown in Fig. 8. The figure shows that for sufficient number of measurements, the NMSE obtained by the proposed technique approaches the NMSE obtained by the Genie-aided techniques. The figure also shows that required number of measurements is a function of the receive SNR. For instance, for a receive SNR of 15 dB and 120 measurements, the NMSE of the proposed technique is similar to the NMSE obtained by the Genie aided technique. As the SNR decreases to 5 dB, more than 200 measurements are required to match the NMSE of the Genie aided technique. To reduce the number of measurements, one can increase the receive SNR by either placing more antennas at the transmitter to increase the array gain or reduce the transmitter-receiver distance to minimize the path-loss.

The success probability, i.e. the probability that the proposed technique successfully detects the locations of the faults, versus the number of antennas for a fixed number of measurements is plotted in Fig. 9. The figure shows that for a fixed number of blockages, the success probability decreases as the number of antennas increases. The figure also shows that the success probability decreases at a faster rate when the number of blockages increases. For instance, for a success probability of 0.9 and  $S = 10$  faulty antennas, 45 measurements are sufficient to successfully detect the faults in an array size of 280 antennas. When the number of faults is increased to  $S = 15$ , the array size reduces to 100 antennas. The reason for this is that CS theory dedicates the number of measurements to scale logarithmically with the length of the sparse vector (array size in this case) and linearly with the support of the sparse vector (the number of blocked antennas). This is optimistic since generally, the number of blocked antennas  $S$  is much lower than the total number of antennas  $N_R$ .

In Figs. 10-12, we assume that both the transmit and receive arrays are subject to random blockages. To analyze the effect

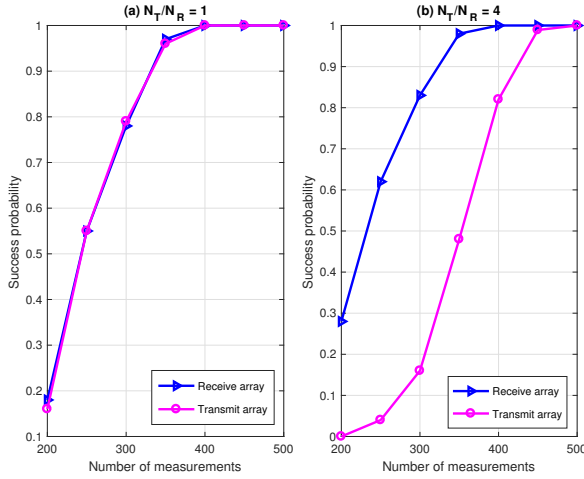


**Fig. 12:** Joint detection of faults in 2D transmit and receive planar arrays all subject to constant blockages;  $P_b = 0.1$  for both arrays,  $[\mathbf{b}_T]_i \in \{0, 1\}$ ,  $[\mathbf{b}]_i \in \{0, 1\}$ , and  $N_T N_R = 1024$ . In (a)  $N_R = 32$ , and  $N_T = 32$ , and in (b)  $N_R = 16$ , and  $N_T = 64$ .

of the number of measurements (or diagnosis time) on the NMSE performance when jointly detecting faults on both the transmit and receive arrays, we plot the NMSE of the technique proposed in Section V and the Genie-aided technique in Fig. 10. For both cases, we observe that the NMSE decreases with increasing number of measurements  $K$ , and for sufficient  $K$ , the NMSE of the proposed technique matches the NMSE obtained by the Genie-aided technique. The figure also shows that the NMSE of the receive array is lower than the NMSE of the transmit array. This is due to the transmit-receive array size difference. For a fixed blockage probability  $P_b$ , larger array sizes encounter more blockages on average, and therefore, require more measurements to detect faults. When the number of antennas is increased, more measurements are required to detect faults as shown in Fig. 11. Unlike the case when the transmit and receive arrays have different sizes, Fig. 11 shows that the NMSE of both the transmit and receive array is similar when the transmit and receive array sizes are fixed and the NMSE decreases with increasing number of measurements.

The success probability when detecting faulty antennas in both the transmit and the receive arrays is plotted in Fig. 12. Fig. 12 (a) shows that for both the transmit and receive array, the success probability increases with increasing number of measurements. Fig. 12 (b) shows that lower number of measurements are required to detect faulty antennas at the receiver when the transmit array size is larger than the receive array size. As the transmit array size increases, the average number of blocked antennas increases as well, thereby requiring more measurements to successfully detect the fault locations.

## VII. CONCLUSIONS

In this paper, we studied the effects of blockages on mmWave linear antenna arrays. We showed that both complete and partial blockages distort the far-field beam pattern of a linear array. Moreover, we showed that partial blockages

result in a higher beam pattern variance when compared to complete blockages. To detect blockages, we proposed two compressed sensing based array diagnosis techniques. The proposed techniques do not require the AUT to be physically removed and do not require any hardware modification. We considered faults at both the receiver and the transmitter. When faults exist at the receiver only, the proposed technique reliably detects the locations of the blocked antennas, if any, and estimates the corresponding attenuation and phase-shift coefficient caused by the blocking particles. When faults exist at both the receive and transmit arrays, the proposed technique jointly detects and estimates blockages at both the receive and transmit arrays. For both cases, the estimated coefficients can be used to calculate new antenna excitations weights to recalibrate the arrays. Due to their reliability and low diagnosis time, the proposed techniques can be used to perform real-time mmWave antenna array diagnosis, and as a result, enhance the mmWave communication links.

## REFERENCES

- [1] F. Boccardi, R. Heath, A. Lozano, T. Marzetta, and P. Popovski, "Five disruptive technology directions for 5G," *IEEE Commun. Mag.*, vol. 52, no. 2, pp. 74-80, Feb. 2014.
- [2] T. Rappaport, R. Heath, R. Daniels, and J. Murdock, *Millimeter wave wireless communications*. Pearson Education, 2014.
- [3] S. Dudzinsky, Jr., *Atmospheric effects on terrestrial millimeter-wave communications*, The Rand Corporation, R-1335-ARPA, March 1974.
- [4] Y. Kuga, F. Ulaby, T. Haddock, and R. DeRoo, "Millimeter-wave radar scattering from snow: 1. Radiative transfer model", *Radio Sci.*, vol. 26, no. 2, pp. 329-341, 1991.
- [5] A. Arage, W. Steffens, G. Kuehnle, and R. Jakoby, "Effects of water and ice layer on automotive radar" in *Proc. of the German Microwave Conf.*, 2006.
- [6] E. Vinyaikin, M. Zinicheva, and A. Naumov, "Attenuation and phase variation of millimeter and centimeter radio waves in a medium consisting of dry and wet dust particles," *Radiophysics and Quantum Electronics*, vol. 37, no. 11, 1994.
- [7] F. Ulaby, T. Haddock, R. Austin, and Y. Kuga, "Millimeter-wave radar scattering from snow: 2. Comparison of theory with experimental observations", *Radio Sci.*, vol. 26, no. 2, pp. 343-351, 1991.
- [8] M. Li and Y. Lu, "Source bearing and steering-vector estimation using partially calibrated arrays," *IEEE Trans. Aerosp. Electron. Syst.*, vol. 45, pp. 1361-1372, Oct. 2009.
- [9] R. Mailloux "Array failure correction with a digitally beamformed array," *IEEE Trans. Antennas Propag.*, vol. 44, no. 12, pp. 1543-1550, Dec. 1996.
- [10] M. Li, M. McGuire, K. S. Ho and G. Hayward, "Array element failure correction for robust ultrasound beamforming and imaging," in *IEEE Ultrasonics Symposium*, San Diego, CA, 2010, pp. 29-32.
- [11] B.-K. Yeo and Y. Lu, "Array failure correction with a genetic algorithm," *IEEE Trans. Antennas Propag.*, vol. 47, no. 5, pp. 823-828, 1999.
- [12] N. Grewal, M. Rattan, and M. S. Patterh, "A linear antenna array failure correction using firefly algorithm," *Progress in Electromagnetics Research*, vol. 27, pp. 241-254, 2012.
- [13] J. Rodriguez, F. Ares, E. Moreno, and G. Franceschetti, "Genetic algorithm procedure for linear array failure correction," *Electronics Letters*, vol. 36, no. 3, pp. 196-198, 2000.
- [14] R. Iglesias, F. Ares, M. Delgado, J. Rodriguez, J. Bregains, and S. Barro, "Element failure detection in linear antenna arrays using case-based reasoning," *IEEE Antennas Propag. Mag.*, vol. 50, no. 4, pp. 198-204, Aug. 2008.
- [15] J. Rodriguez, F. Ares, E. Moreno, and G. Franceschetti, "Genetic algorithm procedure for linear array failure correction," *Electron. Lett.*, vol. 36, no. 3, pp. 196-198, Feb. 2000.
- [16] O. Bucci, M. Migliore, G. Panariello, and G. Sgambato, "Accurate diagnosis of conformal arrays from near-field data using the matrix method," *IEEE Trans. Antennas Propag.*, vol. 53, no. 3, pp. 1114-1120, Mar. 2005.

- [17] J. R.-Gonzalez, F. A.-Pena, M. F.-Delgado, R. Iglesias, and S. Barro, "Rapid method for finding faulty elements in antenna arrays using far field pattern samples," *IEEE Trans. Antennas Propag.*, vol. 57, no. 6, pp. 1679-1683, June 2009.
- [18] A. Buonanno and M. D'Urso, "On the diagnosis of arbitrary geometry fully active arrays," in *the Eur. Conf. Antennas Propag. (EuCAP)*, Barcelona, Apr. 2010.
- [19] M. Migliore, "A compressed sensing approach for array diagnosis from a small set of near-field measurements," *IEEE Trans. Antennas Propag.*, vol. 59, no. 6, pp. 2127-2133, June 2011.
- [20] G. Oliveri, P. Rocca, and A. Massa, "Reliable diagnosis of large linear arrays-Bayesian compressive sensing approach," *IEEE Trans. Antennas Propag.*, vol. 60, no. 10, pp. 4627-4636, Oct. 2012.
- [21] X. Luo, "Robust Large Scale Calibration for Massive MIMO," in *IEEE Global Communications Conference*, San Diego, CA, 2015, pp. 1-6.
- [22] T. Wiese, L. Weiland, and W. Utschick, "DOA estimation and array registration with joint sparse reconstruction methods," in *IEEE 16th Int. Workshop on Signal Processing Advances in Wireless Communications*, Stockholm, 2015, pp. 500-504.
- [23] B. Friedlander and T. Strohmer, "Bilinear compressed sensing for array self-calibration," in *48th Asilomar Conference on Signals, Systems and Computers*, Pacific Grove, CA, 2014, pp. 363-367.
- [24] C. Balanis, *Antenna Theory, Analysis, and Design*, 1997, Wiley.
- [25] M. Wainwright, "Sharp thresholds for high-dimensional and noisy sparsity recovery using  $\ell_1$ -constrained quadratic programming (Lasso)," *IEEE Trans. Inf. Theory*, vol. 55, no. 5, pp. 2183-2202, May 2009.
- [26] M. Akdeniz, Y. Liu, M. Samimi, S. Sun, S. Rangan, T. Rappaport, and E. Erkip, "Millimeter wave channel modeling and cellular capacity evaluation," *IEEE J. on Selected Areas in Commun.*, vol. 32, no. 6, pp. 1164-1179, June 2014.
- [27] E. Candes and Y. Plan, "Near-ideal model selection by  $\ell_1$  minimization," *Ann. Statist.*, vol. 37, pp. 2145-2177, 2009.
- [28] A. Fletcher, S. Rangan, and V. Goyal, "Necessary and sufficient conditions for sparsity pattern recovery," *IEEE Trans. Inform. Theory*, vol. 55, no. 12, pp. 5758-5772, Dec. 2009.
- [29] M. Rudelson and R. Vershynin, "On sparse reconstruction from fourier and gaussian measurements," *Communications on Pure and Applied Mathematics*, vol. 61, pp. 1025-1045, 2008.
- [30] A. Sayed, *Fundamentals of adaptive filtering*, John Wiley & Sons, 2003.
- [31] M. Duarte and R. G. Baraniuk, "Kronecker compressive sensing," *IEEE Trans. Image Process.*, vol. 21, no. 2, pp. 494-504, Feb. 2012.
- [32] R. Horn and C. Johnson, *Topics in Matrix Analysis*, Cambridge University Press, Cambridge, 1991.
- [33] <http://sparselab.stanford.edu>.